Signal enhancement in multiphoton TIRF microscopy by shaping of broadband femtosecond pulses

Richard S. K. Lane,[1,2] Alisdair N. Macpherson,[2] and Steven W. Magennis[1,2,*]

[1]*The School of Chemistry, The University of Manchester, Oxford Road, Manchester, M13 9PL, UK*
[2]*The Photon Science Institute, The University of Manchester, Alan Turing Building, Oxford Road, Manchester, M13 9PL, UK*
steven.magennis@manchester.ac.uk

Abstract: We demonstrate that pulse shaping of a broadband Ti:sapphire laser can result in almost an order of magnitude increase in the sensitivity and signal to background ratio (SBR) of multiphoton total internal reflection fluorescence (TIRF) microscopy. We produced transform-limited pulses of 15 fs duration at the sample, and observed a 8-fold enhancement in the fluorescence of CdSe/ZnS quantum dots via two-photon objective-type TIRF excitation. There was a concomitant 6-fold increase of the SBR upon compression of the pulse duration. Enhancement of non-linear evanescent imaging has recently been demonstrated using surface-plasmons [Opt. Express **17**, 5987 (2009)] and structured substrates [Opt. Express **18**, 23218 (2010)]. Our approach of ultrafast pulse shaping could be used alone or combined with these new methods to offer significant gains in image quality.

OCIS codes: (180.2520) Fluorescence microscopy; (180.4315) Nonlinear microscopy; (300.6410) Spectroscopy, multiphoton; (320.5540) Pulse shaping.

References and links

1. D. Axelrod, "Chapter 7: Total internal reflection fluorescence microscopy," Methods Cell Biol. **89**, 169–221 (2008).
2. D. Axelrod, N. L. Thompson, and T. P. Burghardt, "Total internal inflection fluorescent microscopy," J. Microsc. **129**(1), 19–28 (1983).
3. O. Hollmann, R. Steitz, and C. Czeslik, "Structure and dynamics of α-lactalbumin adsorbed at a charged brush interface," Phys. Chem. Chem. Phys. **10**(10), 1448–1456 (2008).
4. P. Kuhn, K. Eyer, S. Allner, D. Lombardi, and P. S. Dittrich, "A microfluidic vesicle screening platform: monitoring the lipid membrane permeability of tetracyclines," Anal. Chem. **83**(23), 8877–8885 (2011).
5. A. Gunnarsson, L. Dexlin, P. Wallin, S. Svedhem, P. Jönsson, C. Wingren, and F. Höök, "Kinetics of ligand binding to membrane receptors from equilibrium fluctuation analysis of single binding events," J. Am. Chem. Soc. **133**(38), 14852–14855 (2011).
6. C. K. Choi, M. Vicente-Manzanares, J. Zareno, L. A. Whitmore, A. Mogilner, and A. R. Horwitz, "Actin and α-actinin orchestrate the assembly and maturation of nascent adhesions in a myosin II motor-independent manner," Nat. Cell Biol. **10**(9), 1039–1050 (2008).
7. B. Sinha, D. Köster, R. Ruez, P. Gonnord, M. Bastiani, D. Abankwa, R. V. Stan, G. Butler-Browne, B. Vedie, L. Johannes, N. Morone, R. G. Parton, G. Raposo, P. Sens, C. Lamaze, and P. Nassoy, "Cells respond to mechanical stress by rapid disassembly of caveolae," Cell **144**(3), 402–413 (2011).
8. R. Roy, S. Hohng, and T. Ha, "A practical guide to single-molecule FRET," Nat. Methods **5**(6), 507–516 (2008).
9. G. I. Mashanov, D. Tacon, A. E. Knight, M. Peckham, and J. E. Molloy, "Visualizing single molecules inside living cells using total internal reflection fluorescence microscopy," Methods **29**(2), 142–152 (2003).
10. Z. Huang and N. L. Thompson, "Theory for two-photon excitation in pattern photobleaching with evanescent illumination," Biophys. Chem. **47**(3), 241–249 (1993).
11. H. Kano and S. Kawata, "Two-photon-excited fluorescence enhanced by a surface plasmon," Opt. Lett. **21**(22), 1848–1850 (1996).
12. I. Gryczynski, Z. Gryczynski, and J. R. Lakowicz, "Two-photon excitation by the evanescent wave from total internal reflection," Anal. Biochem. **247**(1), 69–76 (1997).

#173710 - $15.00 USD Received 2 Aug 2012; revised 23 Oct 2012; accepted 24 Oct 2012; published 1 Nov 2012

13. F. Schapper, J. T. Gonçalves, and M. Oheim, "Fluorescence imaging with two-photon evanescent wave excitation," Eur. Biophys. J. **32**(7), 635–643 (2003).
14. M. Oheim and F. Schapper, "Non-linear evanescent-field imaging," J. Phys. D **38**(10), R185–R197 (2005).
15. G. L. Duveneck, M. A. Bopp, M. Ehrat, M. Haiml, U. Keller, M. A. Bader, G. Marowsky, and S. Soria, "Evanescent field-induced two-photon fluorescence: excitation of macroscopic areas of planar waveguides," Appl. Phys. B **73**(8), 869–871 (2001).
16. C. Kappel, A. Selle, T. Fricke-Begemann, M. A. Bader, and G. Marowsky, "Giant enhancement of two-photon fluorescence induced by resonant double grating waveguide structures," Appl. Phys. B **79**(5), 531–534 (2004).
17. S. Soria, A. T. K. N, G. Badenes, M. A. Bader, A. Selle, and G. Marowsky, "Resonant double grating waveguide structures as enhancement platforms for two-photon fluorescence excitation," Appl. Phys. Lett. **87**(8), 081109 (2005).
18. D. Ivanov, V. Shcheslavskiy, I. Märki, M. Leutenegger, and T. Lasser, "High volume confinement in two-photon total-internal-reflection fluorescence correlation spectroscopy," Appl. Phys. Lett. **94**(8), 083902 (2009).
19. J. W. M. Chon and M. Gu, "Scanning total internal reflection fluorescence microscopy under one-photon and two-photon excitation: image formation," Appl. Opt. **43**(5), 1063–1071 (2004).
20. W. R. Zipfel, R. M. Williams, and W. W. Webb, "Nonlinear magic: multiphoton microscopy in the biosciences," Nat. Biotechnol. **21**(11), 1369–1377 (2003).
21. R. Bäumner, L. Bonacina, J. Enderlein, J. Extermann, T. Fricke-Begemann, G. Marowsky, and J.-P. Wolf, "Evanescent-field-induced second harmonic generation by noncentrosymmetric nanoparticles," Opt. Express **18**(22), 23218–23225 (2010).
22. R.-Y. He, Y.-D. Su, K.-C. Cho, C.-Y. Lin, N.-S. Chang, C.-H. Chang, and S.-J. Chen, "Surface plasmon-enhanced two-photon fluorescence microscopy for live cell membrane imaging," Opt. Express **17**(8), 5987–5997 (2009).
23. R. Zhang, E. Rothenberg, G. Fruhwirth, P. D. Simonson, F. Ye, I. Golding, T. Ng, W. Lopes, and P. R. Selvin, "Two-photon 3D FIONA of individual quantum dots in an aqueous environment," Nano Lett. **11**(10), 4074–4078 (2011).
24. M. Pawlicki, H. A. Collins, R. G. Denning, and H. L. Anderson, "Two-photon absorption and the design of two-photon dyes," Angew. Chem. Int. Ed. Engl. **48**(18), 3244–3266 (2009).
25. G. S. He, L.-S. Tan, Q. Zheng, and P. N. Prasad, "Multiphoton absorbing materials: molecular designs, characterizations, and applications," Chem. Rev. **108**(4), 1245–1330 (2008).
26. C. Soeller and M. B. Cannell, "Construction of a two-photon microscope and optimisation of illumination pulse duration," Pflügers Arch. Eur. J. Appl. Physiol. **432**, 555–561 (1996).
27. G. Tempea, B. Považay, A. Assion, A. Isemann, W. Pervak, M. Kempe, A. Stingl, and W. Drexler, "Undistorted delivery of sub-15-fs pulses via high-numerical-aperture microscope objectives," Proc. SPIE **6442**, 64420P, 64420P-5 (2007).
28. A. M. Larson and A. T. Yeh, "Ex vivo characterization of sub-10-fs pulses," Opt. Lett. **31**(11), 1681–1683 (2006).
29. I. Pastirk, J. M. Dela Cruz, K. A. Walowicz, V. V. Lozovoy, and M. Dantus, "Selective two-photon microscopy with shaped femtosecond pulses," Opt. Express **11**(14), 1695–1701 (2003).
30. P. Xi, Y. Andegeko, L. R. Weisel, V. V. Lozovoy, and M. Dantus, "Greater signal, increased depth, and less photobleaching in two-photon microscopy with 10 fs pulses," Opt. Commun. **281**(7), 1841–1849 (2008).
31. P. Xi, Y. Andegeko, D. Pestov, V. V. Lovozoy, and M. Dantus, "Two-photon imaging using adaptive phase compensated ultrashort laser pulses," J. Biomed. Opt. **14**(1), 014002 (2009).
32. D. Axelrod, "Selective imaging of surface fluorescence with very high aperture microscope objectives," J. Biomed. Opt. **6**(1), 6–13 (2001).
33. L. S. Natrajan, A. Toulmin, A. Chew, and S. W. Magennis, "Two-photon luminescence from polar bis-terpyridyl-stilbene derivatives of Ir(III) and Ru(II)," Dalton Trans. **39**(45), 10837–10846 (2010).
34. R. Pantoja, E. A. Rodriguez, M. I. Dibas, D. A. Dougherty, and H. A. Lester, "Single-molecule imaging of a fluorescent unnatural amino acid incorporated into nicotinic receptors," Biophys. J. **96**(1), 226–237 (2009).
35. U. Resch-Genger, M. Grabolle, S. Cavaliere-Jaricot, R. Nitschke, and T. Nann, "Quantum dots versus organic dyes as fluorescent labels," Nat. Methods **5**(9), 763–775 (2008).
36. B. Mahler, P. Spinicelli, S. Buil, X. Quelin, J.-P. Hermier, and B. Dubertret, "Towards non-blinking colloidal quantum dots," Nat. Mater. **7**(8), 659–664 (2008).
37. T. Ridler and S. Calvard, "Picture thresholding using an iterative selection method," IEEE Trans. Syst. Man Cybern. **SMC-8**, 630–632 (1978).
38. V. V. Lozovoy and M. Dantus, "When shorter is better," in "Commercial and biomedical applications of ultrafast lasers IX," Proc. SPIE **7203**, 72030Y, 72030Y-7 (2009).
39. W. Wang, Y. Liu, P. Xi, and Q. Ren, "Origin and effect of high-order dispersion in ultrashort pulse multiphoton microscopy in the 10 fs regime," Appl. Opt. **49**(35), 6703–6709 (2010).
40. M. Müller, J. Squier, R. Wolleschensky, U. Simon, and G. J. Brakenhoff, "Dispersion pre-compensation of 15 femtosecond optical pulses for high-numerical-aperture objectives," J. Microsc. **191**(2), 141–150 (1998).
41. Y. Andegeko, D. Pestov, V. V. Lozovoy, and M. Dantus, "Ultrafast multiphoton microscopy with high-order spectral phase distortion compensation," Proc. SPIE **7183**, 71830W, 71830W-6 (2009).
42. S. Weiss, "Measuring conformational dynamics of biomolecules by single molecule fluorescence spectroscopy," Nat. Struct. Biol. **7**(9), 724–729 (2000).

#173710 - $15.00 USD Received 2 Aug 2012; revised 23 Oct 2012; accepted 24 Oct 2012; published 1 Nov 2012

43. K.-C. Chiu, C.-Y. Lin, C. Y. Dong, and S.-J. Chen, "Optimizing silver film for surface plasmon-coupled emission induced two-photon excited fluorescence imaging," Opt. Express **19**(6), 5386–5396 (2011).
44. Y. Silberberg, "Quantum coherent control for nonlinear spectroscopy and microscopy," Annu. Rev. Phys. Chem. **60**(1), 277–292 (2009).
45. D. Brinks, R. Hildner, F. D. Stefani, and N. F. van Hulst, "Beating spatio-temporal coupling: implications for pulse shaping and coherent control experiments," Opt. Express **19**(27), 26486–26499 (2011).

1. Introduction

Evanescent wave imaging in the form of total internal reflection fluorescence (TIRF) microscopy is a powerful tool in the physical and life sciences [1]. This widefield technique allows fluorophores within around 100 nm of a refractive index boundary to be detected, even in the presence of significant background fluorescence in the bulk sample. It is used to image surfaces [2], interfaces [3], liposomes [4, 5], and cells [6, 7], and can probe the structure and dynamics of such systems down to the single-molecule level [8, 9]. TIRF studies to date have been performed almost exclusively using resonant excitation.

The concept of an evanescent field generated via two-photon (2P) excitation combined with TIRF was first discussed in 1993 [10], while the first experiments were reported soon after [11, 12]. Oheim et al. provided a theoretical framework for non-resonant TIRF, and described imaging of cells using a range of TIRF geometries [13, 14]. Marowsky et al. combined 2P excitation with planar waveguides to give large signal enhancements [15–17], while Ivanov et al. combined non-resonant TIRF with fluorescence correlation spectroscopy [18]. A variant of non-linear TIRF using a scanned evanescent field has also been implemented [19].

The possible advantages of non-resonant excitation for TIRF include a reduction of background fluorescence generated in the sample and optical elements (since the spatial concentration of photons is too low to excite fluorescence outside of the focal volume), reduced photobleaching, less scattering from the longer wavelength incident beam (e.g. at refractive index boundaries), greater spectral separation of excitation and emission, transmission of the excitation beam through opaque substrates, and the possibility of simultaneous excitation of multiple fluorophores. In spite of this, non-resonant TIRF has not been widely adopted as a widefield analogue of far-field multiphoton microscopy [20].

A number of recent reports illustrate that non-resonant TIRF has the potential for a wider range of applications. Marowsky et al. demonstrated that the use of structured waveguides enabled non-linear second-harmonic generation imaging [21]. The group of Chen demonstrated significant enhancements in fluorescence emission by exciting surface plasmons (SP) at a thin Ag film/dielectric interface [22]; importantly, this study demonstrated that 2P imaging actually produced brighter images than one photon (1P) imaging of cell samples. Finally, a recent report described the use of 2P TIRF for super-resolution imaging, which involved determination of the centre of the point spread function of single quantum dots (Q-dots) [23].

The efficiency of multiphoton excitation is a product of the multiphoton absorption cross section and the temporal and spatial photon concentration. The last decade has witnessed a huge growth in the development of new molecules tailored for multiphoton processes, so the absorption cross section is no longer a limiting factor [24, 25]. However, the dispersion introduced by the multiple optical elements used in multiphoton microscopy setups, and the need to study samples in complex inhomogeneous environments, means that the laser pulse at the objective focus usually becomes highly broadened and distorted, greatly reducing the signal intensity. This is potentially a major obstacle to non-resonant imaging using ultrashort laser pulses, unless pre-compensation correction techniques are used to restore the pulse duration close to the transform limit.

In far-field setups utilising ca. 100 fs pulse durations, prism-pair compressors are commonly used to correct the second-order dispersion (SOD), or chirp [26]. However, if one of the new generation of ultrabroad-bandwidth Ti:sapphire oscillators that can support pulse

#173710 - $15.00 USD Received 2 Aug 2012; revised 23 Oct 2012; accepted 24 Oct 2012; published 1 Nov 2012

durations of ca. 10 fs is to be optimally used as the excitation source, then more sophisticated approaches are required to additionally pre-compensate for the higher order dispersion terms (such as third-order dispersion, TOD), which become significant as the pulse duration decreases [27]. Multiple reflections from highly dispersive chirped mirrors designed to provide negative SOD and TOD have been used to obtain ~12 fs pulses at the focal plane [28]. Using a 4*f* pulse shaper and the multiphoton intrapulse interference phase scan (MIIPS) method to detect and compensate the spectral phase of the pulse [29], Dantus et al. were able to adaptively shape pulses, delivering transform limited (TL) 10 fs pulses at the focus of a high numerical aperture (N.A.) objective used for 2P-excitation fluorescence microscopy, with significant gains in signal [30, 31].

Until now, the combination of pulse shaping and TIRF was unexplored. We show here that pre-compensating for pulse-phase distortions in multiphoton TIRF using a MIIPS-enabled pulse shaper results in a signal enhancement of almost an order of magnitude. We also demonstrate that single quantum dot (Q-dot) emitters with modest two-photon cross sections of only 1200 GM (Goeppert-Mayer, 1 GM = 10^{-50} cm^4 s $photon^{-1}$) can be detected. The ability to generate transform-limited (TL) pulses at the sample should enable the wider application of multiphoton TIRF.

2. Methods and materials

2.1 Pulse-shaped multiphoton TIRF

A schematic of the experimental setup is shown in Fig. 1. The excitation source was a broadband Ti:sapphire oscillator (Mantis, Coherent) producing pulses of 560 mW average power with a FWHM bandwidth of 97 nm centred at 796 nm (measured using a fibre-coupled spectrometer: USB4000, Ocean Optics). The pulse duration measured with a scanning autocorrelator (PulseCheck-50 with short pulse and FROG options, APE) before and after the telescope used to expand the beam to a ~3 mm diameter was 68 fs (Gaussian fit) and 121 fs, respectively. The laser output pulse was compressed to 15 fs with a compact pulse compressor (CPC, Coherent), which uses a negative dispersion mirror (NDM) pair and a thin sliding wedge to compensate for variable amounts of SOD. The beam then enters a low-loss LCD-based 4*f* pulse shaper (Silhouette, Coherent) that uses a 128 pixel dual array liquid crystal spatial light modulator (SLM) to perform spectral phase and amplitude modulation. After further beam expansion, the beam was reflected from a dichroic mirror (DC1: 675DCSPXR, Chroma) onto a high N.A. objective (Nikon Plan Apo TIRF 60 × , N.A. = 1.45), which is required to achieve the TIR condition [32]. After reaching the objective plane, the pulse duration had broadened to 250 fs (FWHM) and was no longer Gaussian, and the spectral bandwidth had decreased to 70 nm, as measured using MIIPS. Further adjustment of the NDM pair did not yield significant compression as this only compensated for SOD, and may have introduced higher order dispersion (HOD) at the objective plane.

#173710 - $15.00 USD Received 2 Aug 2012; revised 23 Oct 2012; accepted 24 Oct 2012; published 1 Nov 2012

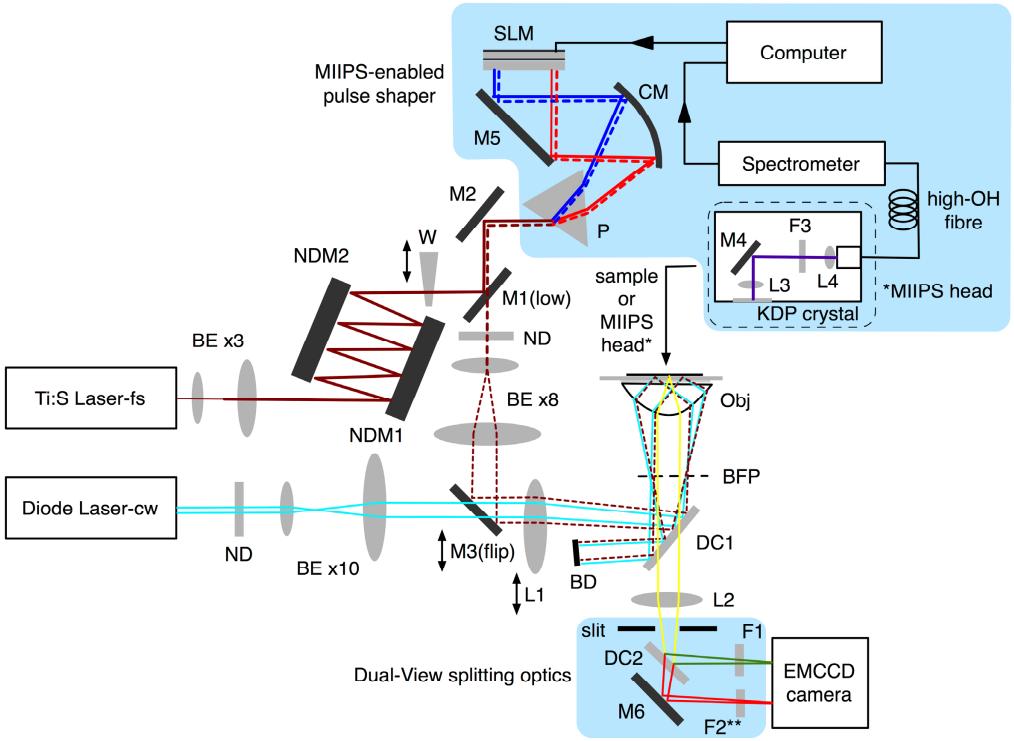

Fig. 1. Schematic representation of the objective-type TIRF microscope with 1P and 2P excitation. L1-L4: lenses, NDM1-2: negative dispersion mirrors, BE: beam expander, BD: beam dump, W: wedge, P: prism, ND: neutral density filters CM: concave mirror, SLM: dual (reflective) spatial light modulator, BFP: back focal plane, Obj: microscope objective, M1-4: protected silver mirrors, M5-M6: dielectric mirrors, DC1-2: dichroic filter, F1-2: bandpass filter (**F2 path blocked), cyan/magenta/red/blue lines: laser light, yellow/green/red lines: fluorescence. See text for details.

The fluorescence was collected by this same objective, through the dichroic, and was imaged by an EMCCD camera (Evolve 512, Photometrics) and dual-channel imaging device (DV2, Photometrics) with a dichroic mirror (DC2: 595DCXR) and barrier filter (F1:525/50 nm). Note that the second imaging channel (M6 and F2) was blocked for this work. Protected silver mirrors (MCUO, Biophotonic Solutions) were used to steer the beam post shaping; these were specified to be dispersion-free (group delay = 0 fs) across the wavelength range of the fundamental laser spectrum.

Phase distortions at the sample plane were corrected using the MIIPS method for second harmonic generation (SHG) [29]. To create SHG, an ultra thin 10 µm thick KDP crystal (MDU-1, Biophotonics Solutions) was mounted perpendicularly to the objective turret. Using the manual focusing drive of the microscope it was brought within 100 µm of the front element of the 60 × TIRF objective lens. By mounting the crystal housing on a micrometer-controlled translation stage, the frequency-doubled beam of 350-450 nm was steered through an aspheric lens (f = 0.284, w.d = 1.6 mm, N.A. = 0.67) and coupled into a 200 µm core diameter UV-VIS fibre. A BG-39 filter separated the SHG from the fundamental laser beam. A spectrometer configured with a 25 µm slit and 1.2 N.A. collection lens monitored the SHG signal intensity. A series of reference functions were applied at the Fourier plane of the reflective SLM-based pulse shaper to maximise the SHG signal and therefore obtain TL pulses at the sample by full phase correction. The FWHM pulse duration was found to change from 250 fs (T/T_{TL} = 16.8) uncorrected to 15.5 fs (T/T_{TL} = 1.029) after removing the majority of spectral phase distortions; T/T_{TL} is the ratio of the measured pulse duration (T) to the

#173710 - $15.00 USD Received 2 Aug 2012; revised 23 Oct 2012; accepted 24 Oct 2012; published 1 Nov 2012

theoretical time duration (T_{TL}) for a Gaussian-shaped pulse with a flat spectral phase across the spectrum. It was found that the uncompensated pulse had an irregular, non-Gaussian form possibly due to a minor alignment issue. Therefore the ratio of the two FWHM measurements is only an estimate of the true pulse duration gain factor. The MIIPS method utilized here is designed for use in a far-field epifluorescence configuration (with the laser beam aligned to the optical axis). Therefore, the beam was translated back to a TIR configuration after the MIIPS measurement, which could potentially alter the dispersion, in comparison with far field imaging. To check the effect of moving to the near-field configuration, small amounts of SOD and TOD were added to the TL profile generated in the far field. It was found, by iteration, that addition of SOD alone (625 fs^2) allowed the signal in a TIR configuration to be maximised (Fig. 2). This far- to near-field tuning procedure is quick and unchallenging compared to the, often complex, fine alignment required when using combinations of optical elements to compensate multiple orders of dispersion without MIIPS.

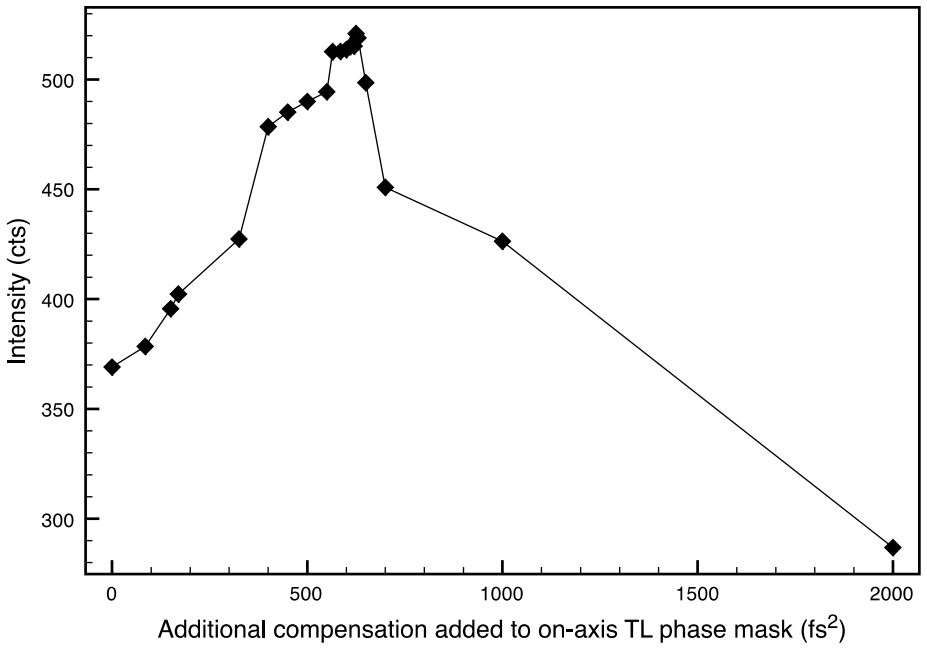

Fig. 2. Variation in fluorescence from Q-dots in "off-axis" TIRF configuration upon applying varying amounts of compensation "on axis." See text for details.

As controls, data were also recorded for blank surfaces and with the laser in CW mode, to ensure that emission resulted from non-linear excitation. Background signal from the instrument (e.g. the objective lens) was negligible with non-resonant excitation. No damage to the objective lens was observed using pulse energies up to 1.5 nJ (unfiltered maximum power at the objective entrance of 120 mW, 80 MHz).

2.2 Two-photon spectroscopy and cross section measurement

To record 2P emission spectra of the Q-dots, a beam from the Mantis laser was passed through a dichroic mirror (650DCSPXR, Chroma), and focused with a 40 × objective lens (PF, N.A. = 0.60, Nikon) onto the sample, which was in a 1 cm pathlength cuvette. The incident power was monitored throughout (Solo meter and PH100-Si head, Gentec). The sample fluorescence was collected by the same objective, reflected from the dichroic mirror, passed though a shortpass filter (625SP, Chroma) to remove residual excitation light and detected by a fibre-coupled spectrometer (QE6500-FL, Ocean Optics). The 2P cross section

#173710 - $15.00 USD Received 2 Aug 2012; revised 23 Oct 2012; accepted 24 Oct 2012; published 1 Nov 2012

was measured by comparing spectra of the Q-dots in toluene (*ca.* 500 nM) to those of a standard, rhodamine B in methanol, as described previously [33].

2.3 One-photon spectroscopy and TIRF

An externally-doubled diode solid-state laser (Cyan-Scientific, Spectra Physics) of linewidth <1 MHz and M2 <1.1 operating at 50 mW CW was used for 1P excitation at 488 nm (Fig. 1). The beam was reflected, and fluorescence collected, by replacing DC1 with a 491RDCXT dichroic filter. The unfiltered maximum power at the objective entrance was 1.1 mW (~190 mW/cm^2), comparable in magnitude to other single molecule studies [34]. To ensure the 1P and 2P beams were collinear, the final mirror in each beam path was mounted with micrometer adjustment perpendicular to the beam. The 1P excitation beam was expanded by an appropriate amount to yield comparable spot size as for 2P excitation on the objective back focal plane (BFP), and hence comparable active fields of view (FOV). Bulk absorption and emission spectra of toluene solutions were recorded on an absorption spectrophotometer (Lambda-1050, Perkin-Elmer) and spectrofluorometer (Fluorolog FL3-iHR, Horiba), respectively.

2.4 Materials

Highly dilute solutions of CdSe/ZnS (core/shell) Q-dots (λ_{max} = 530 nm, PlasmaChem) in toluene (ACS grade, Sigma-Aldrich) were drop-cast onto a cleaned glass surface, and immobilised by evaporation of the solvent.

3. Results

To test the effects of pulse shaping on multiphoton TIRF, we used CdSe Q-dots, which are photostable emitters [35]. Figure 3 shows the absorption and emission spectra (following excitation at 800 nm) of a solution of the Q-dots in toluene. As can be seen, there is essentially no absorption above 540 nm. The intensity of the multiphoton emission also obeys a power-squared law, indicating a 2P excitation mechanism is predominant (Fig. 3 inset). The same emission peak at 530 nm is observed for resonant excitation at 488 nm. We deposited highly dilute solutions of 530 nm Q-dots in toluene onto a cleaned glass surface to generate a low concentration of single nanoparticles and nanoparticle aggregates. Samples were excited via widefield TIRF microscopy using the setup in Fig. 1.

#173710 - $15.00 USD Received 2 Aug 2012; revised 23 Oct 2012; accepted 24 Oct 2012; published 1 Nov 2012

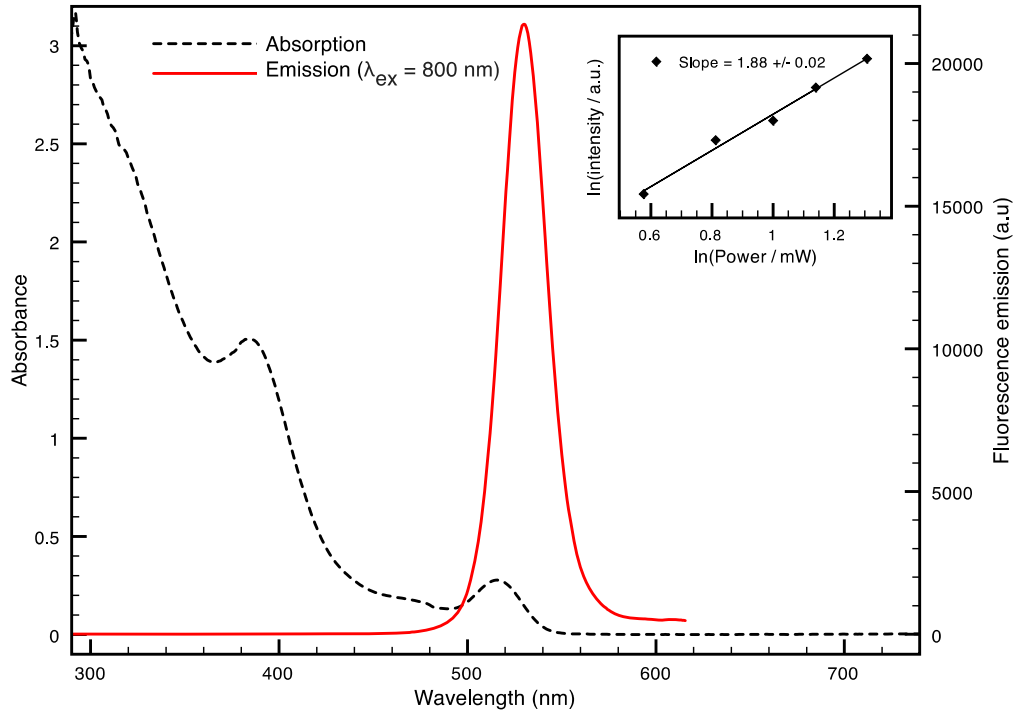

Fig. 3. Absorption and ensemble fluorescence spectra of Q-dots. The inset shows that excitation at 800 nm obeys a power squared law, as expected for a 2P process.

Figures 4(a) and 4(b) demonstrate that switching from uncompensated [Fig. 4(a)] to shaped [Fig. 4(b)] 2P-TIRF, resulted in significant enhancement of emission from the same nanoparticles. From Fig. 3, it is clear that resonant excitation is not possible with the infrared laser. Furthermore, switching the Ti:sapphire laser to CW mode, with similar average power, resulted in the complete disappearance of Q-dot fluorescence, indicative of non-resonant excitation. Signals from both nanoaggregates and single Q-dots were detected. The signals labeled 1-3 in Fig. 4(b) were from single nanoparticles. The individual Q-dots were identified by their stochastic blinking behaviour, following 1P excitation, as shown in Fig. 4(c). These traces exhibited a range of intensities in the on state, as observed previously [36]. Note that without shaping, these individual particles were not observed [Fig. 4(a)].

The effect of pulse shaping on the Q-dot emission is presented in more detail in Fig. 5. Figures 5(a) and 5(b) show 2D and 3D plots, respectively, of the same Q-dot nanoaggregates before and after shaping. The incident laser power differed by a factor of × 1.46 between shaped and uncompensated excitation pulses, which we attribute to minor changes in the beam profile. The images are therefore scaled to account for this power difference (assuming a power-squared dependence). As spatial dispersion of the beam was achieved using a prism, rather than laser source-matched diffraction gratings, it was only possible to fill 80% of the SLM pixel array. This may explain the small amount of uncorrected phase in the shaped pulse [Fig. 5(c)].

#173710 - $15.00 USD Received 2 Aug 2012; revised 23 Oct 2012; accepted 24 Oct 2012; published 1 Nov 2012

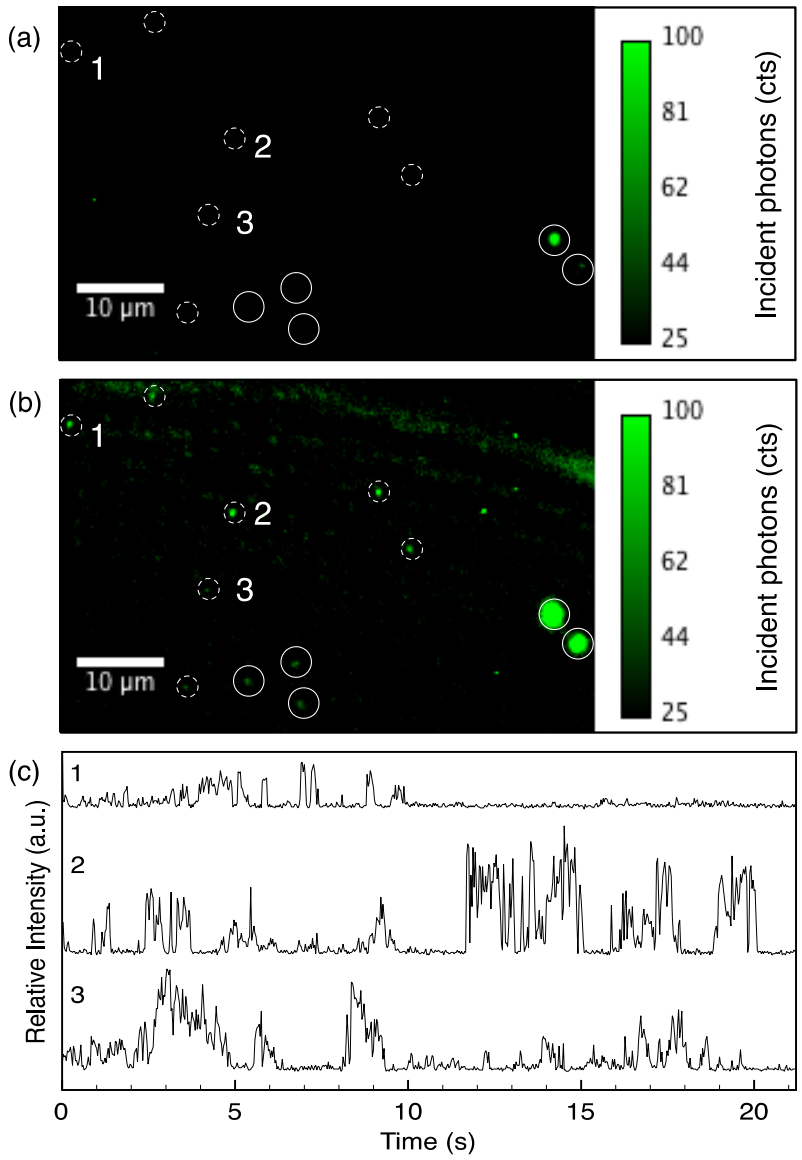

Fig. 4. Shaped versus uncompensated 2P TIRF. Fluorescence images show the same single and aggregated CdSe/ZnS Q-dots evaporated onto a clean surface before and after shaping. Dashed white circles indicate single particles, solid white circles indicate nanoaggregates. A single frame from each data set is shown. (a) 2P uncompensated excited sample, integration time of 300 s. (b) 2P shaped excited sample, integration time of 300 s. (c) time traces of the single particles indicated in 4(a) and 4(b) measured with 1P excitation (integration time 33 ms). Field striations are observable in the FOV of 4(b).

#173710 - $15.00 USD Received 2 Aug 2012; revised 23 Oct 2012; accepted 24 Oct 2012; published 1 Nov 2012

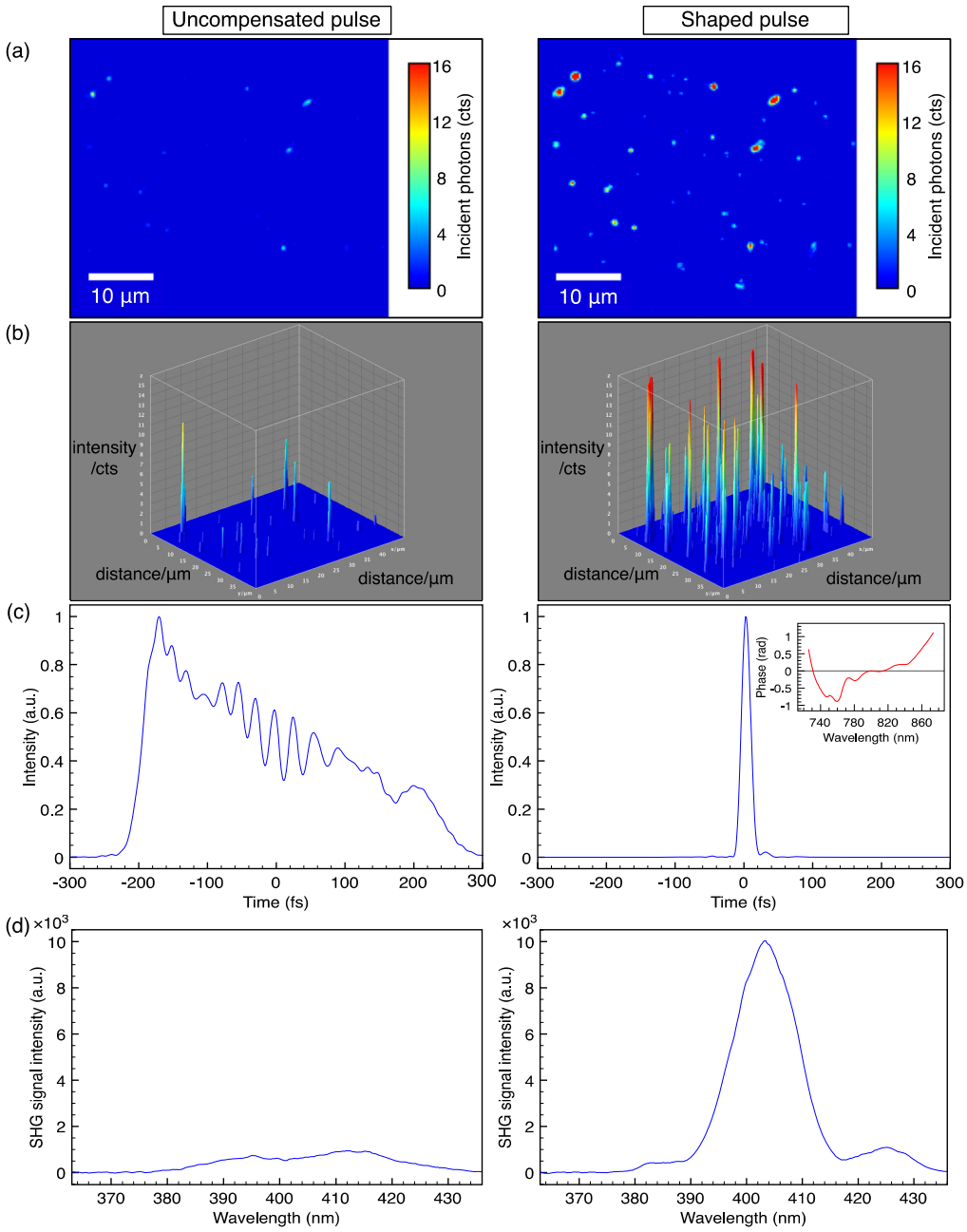

Fig. 5. Fluorescence from immobilised CdSe/ZnS Q-dot nanoaggregates observed by 2P TIRF microscopy. (a)-(b) 2D and 3D surface intensity plots (photoelectrons measured) where each frame is the average of 500 exposures at 10 Hz. The intensity axes are scaled to a dynamic range of 0-16 cts to provide the best visual contrast, and facilitate comparison. The plots are also normalised to the same incident excitation power of 120 mW. The imaged area is 42 by 47 µm. (c) Excitation pulse-widths for applied phase compensation mask measured in epifluorescence configuration, estimated at 250 fs for uncompensated pulses, and 15 fs for shaped pulses, assuming Gaussian profiles. Inset: residual phase for the TL pulse (d) SHG spectrum measured in epifluorescence configuration.

To allow a relative comparison, all signal measurements were normalised to incident counts per second per watt of excitation power (cts/s/W) as shown in Table 1. To avoid

#173710 - $15.00 USD Received 2 Aug 2012; revised 23 Oct 2012; accepted 24 Oct 2012; published 1 Nov 2012

selection bias, both images were thresholded separately with the commonly used isodata algorithm [37], and the generated masks applied to both uncompensated and shaped images to define regions of interest containing nanoaggregates. The average intensity per pixel over these extracted regions of interest was measured with floating point precision for each image composite. Due to the overlapping point spread functions around each aggregate structure, boundaries between the low edge of the signal region and background regions are not well defined as a mixture of two Gaussian functions. Therefore thresholding to locate background regions was carried out manually, ensuring the selected data had counts well separated from signal values.

The shaped signal was found to be enhanced by a factor of ~8 compared to the uncompensated signal. This net gain in the evanescent field is comparable to that measured previously in the far field at the focus of a high N.A. objective [38]. The similar increase for all particles shows that the stochastic blinking observed in Fig. 4(c) is not affecting the result, as expected due to the long integration time. A 10-fold increase in the peak intensity of SHG emission from the KDP crystal was also measured [Fig. 5(d)]. The shaped background was found to be larger than the uncompensated background by a factor of ~1.5. A proportion of the background is due to autofluorescence from impurities in or on the glass slide, the sample, and within the objective lens elements. Given the higher peak power obtained by shaping, it is expected that the background will also rise upon pulse compression. A quantitative measurement of enhancement was made using the signal-to-background ratio (SBR) for our particular setup, where the signal is defined as the sum of the sample and background intensities (Table 1). Overall the SBR for uncompensated pulses was 100, and for shaped pulses was 560, a 6-fold enhancement. The SBRs for single Q-dots are also included in Table 1; these were calculated from the average signal and background intensities in Fig. 4. The low signal intensity from the single Q-dots with uncompensated pulses precluded a comparison of SBR before and after shaping.

Table 1. Comparison of Signal, Background, and SBR for Compensated and Uncompensated Multiphoton TIRF Images of Nanoaggregates and Single Quantum Dots*

Sample type	Excitation mode	Signal (cts/s/W)	Background (cts/s/W)	SBR
nanoaggregates	2P shaped	2.8×10^2	0.50	560
nanoaggregates	2P uncompensated	33	0.33	100
single Q-dots	2P shaped	4.8	1.6	3.0
single Q-dots	2P uncompensated	1.1	1.1	1.0

*Note that the nanoaggregate and single Q-dot data were recorded on different days, hence the differences in absolute background signal. For uncompensated excitation, the signal was too weak to detect single Q-dots.

4. Discussion

We have combined ultrafast pulse shaping with multiphoton TIRF for the first time. In order to assess the potential of pulse-shaped 2P TIRF for fluorescence imaging, we used immobilised CdSe Q-dots, which were chosen for their photostability and reasonable two-photon cross section. Pulse shaping can compensate for the many distortions introduced by optical components so that a short pulse duration can be delivered to the sample. For example, the multiple elements of a typical high N.A. objective, an essential component in most imaging systems, will stretch a 20 fs pulse to beyond 100 fs by a combination of SOD and higher-order dispersions (HOD) [39, 40]. We corrected these distortions at the sample plane with MIIPS using a SHG signal as the input. For pulses of ≥ 100 nm spectral bandwidth, MIIPS can correct dispersion up to fifth order making it superior to other methods, which only correct SOD or TOD [26–28, 41]. We were able to produce a TL pulse of 15 fs at the sample in a multiphoton TIRF setup, resulting in almost an order of magnitude increase in signal and SBR. The observed magnitude of improvement was less than the 16-fold enhancement expected for an inverse linear relationship between pulse duration and

#173710 - $15.00 USD Received 2 Aug 2012; revised 23 Oct 2012; accepted 24 Oct 2012; published 1 Nov 2012

signal intensity. However, as discussed, the uncompensated pulses were non-Gaussian and irregularly shaped so a more complex relationship exists.

In principle, the emission of any emitter can be enhanced using pulse-shaped multiphoton TIRF. Enhancements even greater than those reported here could be obtained, depending on the complexity of the optical system and the sample environment. The signal enhancement also translates into an effective corresponding increase in the temporal resolution for the study of dynamic processes [42]. As discussed, exciting surface plasmons (SP) at a thin Ag film/dielectric interface significantly enhances the SBR of TIRF images of cell samples [22, 43]. In addition, structured substrates can result in large enhancements in fluorescence and SHG [21]. Pulse shaping is compatible with both of these approaches, offering the potential for further increases in sensitivity and SBR; alternatively, the same signal may be achieved with lower excitation powers, which would be beneficial for samples that photobleach.

Finally, our approach opens up the possibility of producing more complex pulse shapes with non-linear TIRF, rather than simply using transform-limited pulses. One exciting application could be the development of widefield coherent control. In this case, the goal would not be to produce TL pulses, but to instead tailor the pulse shape, in order to steer the molecules towards a particular excited state pathway [44]. Although not used in this study, we have also implemented combined amplitude and phase shaping. By applying a Gaussian function to the amplitude mask and adding a polynomial pattern to the phase mask calculated for TL pulses, a series of broadening Gaussian-shaped pulses at the objective were created. This level of shaping control would enable exploration of coherent dynamics. In this context, it has recently been shown that the performance of pulse shapers can be optimized for such experiments [45]. The development of advanced ultrafast laser technology continues unabated, with rapid improvements in ease of use, and reductions in cost. Thus, pulse-shaped multiphoton TIRF microscopy could find the widespread use of its far field counterpart.

Acknowledgments

We thank Haowen Li, Igor Pastirk and Dmitry Pestov (Biophotonics Solutions) for advice with the MIIPS setup, Max Kolff (Ocean Optics) for the loan of a fibre-coupled spectrometer, and Nigel Scrutton for the loan of the EMCCD camera. The laser and diagnostic equipment are PSI central facilities. SWM acknowledges the award of an EPSRC advanced research fellowship (EP/D073154).

#173710 - $15.00 USD Received 2 Aug 2012; revised 23 Oct 2012; accepted 24 Oct 2012; published 1 Nov 2012